into the molecular mechanism of ADAMs' target recognition, which ADAMs shed which key substrates in specific biological events. Since ADAMs are potential therapeutic targets, the distinct surface feature created by the HVR of the individual ADAMs might also provide insights into the future design of drugs with higher specificity for each member of ADAMs. We suggest that the HVR, not the disintegrin domain, should be the focus of searches for physiological targets of ADAMs.

Materials and methods

Protein preparation and crystallization

The details of the preparation, crystallization and preliminary X-ray analysis of VAP1 will be described elsewhere (T Igarashi *et al*, in preparation). VAP1 was isolated from the crude snake *Crotalus atrox* venom (Sigma-Aldrich, USA) and subjected to sitting- or hanging-drop vapor diffusion crystallization. Two distinct crystal forms ($P2_12_12_1$ and $P4_12_12$) were obtained with the reservoir solution containing 15% polyethyleneglycol 8000 and 100 mM sodium cacodylate at pH 6.5, with (orthorhombic form) or without (tetragonal form) 20 mM cobaltous chloride hexahydrate. GM6001-bound crystals were prepared by adding GM6001 (CALBIOCHEM) to the drop with the orthorhombic crystal at a final concentration qof 0.33 mM (twice the protein concentration) followed by a 12-h incubation. Crystals were flash-frozen under the nitrogen flow at 90 K.

Diffraction data collection

All the diffraction data were collected at SPring-8 beamlines using either ADSC quantum 310R CCD (for the inhibitor-bound crystal at the beamline BL41XU with $\lambda = 1$ Å), Rigaku *R*-axis V imaging plate (for orthorhombic native crystal at the beamline BL45PX with $\lambda = 1$ Å) or Jupitor CCD (for the tetragonal crystal at the beamline BL45PX with $\lambda = 0.98$ Å) detectors at 90 K. The images were reduced using HKL2000. Both orthorhombic and tetragonal native data sets were collected to 2.5-Å resolution and inhibitor-bound crystal data sets were collected to 3.0 Å resolution (Table I).

Structural analysis

All structures were solved by the molecular replacement method by MOLREP in the CCP4 suite (CCP4, 1994) by using acutolysin-C (1QUA) (Zhu *et al*, 1999) as a starting model. Initially, the MR solution obtained from the orthorhombic crystal data set, assumed two M-domains in the asymmetric units. After manual rebuilding by TURBO-FRODO, the model was subjected to tortional molecular dynamic refinements with restrained NCS averaging of the M-domains using CNS (Brunger *et al*, 1998) and iterative refinements and manual rebuilding of the model improved the electron-density map and enabled us to extend the model. First, we found the electron densities associated with the pieces of helical segments of the molecules and modelled them as poly-alanine chains. After cycles of refinements, we assigned those segments as the parts of helices H7 and H8, where the secondary structures are predicted to be helices, judging from the electron densities associated with the side chains. At this stage, four tyrosine residues, Tyr575 and Try576 within the central β strands of the HVRs were clearly defined, and we noticed that there was another NCS-axis between the C-domains. After iterative rounds of refinements with restrained NCS averaging of the C-domains and manual model building, we completed modelling of the C-domains. From this stage onward, no NCS averaging was included in the refinements. Next, we modelled the D-domains with the help of automated chain tracing using the program ARP/wARP (Perrakis *et al*, 1999) and with the structural model of trimestatin (1J2L) as a guide. After completely modelling the polypeptide chains, we noticed that isolated lobes of high electron densities surrounded by oxygen atoms occurred both in the D_x- and D_z-domains. For these sites, calcium ions fit optimally to the electron density with a refined occupancy of 100% and reasonably low *B*-values, thus, we included calcium ions in the model. We also assigned a cobalt ion, which was supplemented in the crystallization buffer for the orthorhombic crystal form, located between the M- and D_x-domains in the A molecule. The part of the carbohydrate chain linked to residue Asn218 (two *N*-acetylglocosamine (NAG) moieties) was modelled. Then, water molecules were assigned. The *VAP1* cDNA encodes a protein with 610 amino-acid residues; however, the N-terminus is processed by post-translational modification (Masuda *et al*, 1998, 2000). Here, protein sequencing of the de-blocked VAP1 molecule clarified that the Glu184 side chain was modified into a pyro-form. The electron densities associated with almost the entire molecule except for the first pyroglutamic acid were defined in either monomer within the orthorhombic crystal. In the final model, 86.1% of the residues lay in the most favorable region, 13.3% in the additionally allowed region and 0.7% in the generously allowed region of the Ramachandran plot. The tetragonal crystal and inhibitor-bound crystal were solved by MR with the domains of the refined orthorhombic apo-form as a starting model. In the final model, 83.6% (80.6%) of the residues lay in the most favorable region, 15.7% (18.9%) in the additionally allowed region and 0.7% (0.5%) in the generously allowed region for tetragonal (inhibitor-bound) crystals in the Ramachandran plot. In either crystal form, the asymmetric unit contained one dimer molecule. All six monomers had almost identical structures. Refinement statistics are shown in Table I.

PDB accession codes

Atomic coordinates and structure factors have been deposited in the Protein Data Bank under accession codes 2ERO, 2ERP and 2ERQ for the orthorhombic native, GM6001-bound form and tetragonal-form, respectively.

Supplementary data

Supplementary data are available at *The EMBO Journal* Online.

Acknowledgements

We thank Yuko Oishi and staff in SPring-8 beamlines for assistance with data acquisition and Junichi Takagi for discussions and critical reading of the manuscript. This work was partly supported by Grant nano-001 for Research on Advanced Medical Technology from the Ministry of Health, Labor, and Welfare of Japan, and by grants from the Takeda Science Foundation, from the Kao Foundation for Arts and Science and from Senri Life Science Foundation. The authors declare no competing financial interests.

References

Almeida EA, Huovila AP, Sutherland AE, Stephens LE, Calarco PG, Shaw LM, Mercurio AM, Sonnenberg A, Primakoff P, Myles DG, White JM (1995) Mouse egg integrin alpha 6 beta 1 functions as a sperm receptor. *Cell* **81:** 1095–1104

Becherer JD, Blobel CP (2003) Biochemical properties and functions of membrane-anchored metalloprotease-disintegrin proteins (ADAMs). *Curr Top Dev Biol* **54:** 101–123

Black RA, Rauch CT, Kozlosky CJ, Peschon JJ, Slack JL, Wolfson MF, Castner BJ, Stocking KL, Reddy P, Srinivasan S, Nelson N, Boiani N, Schooley KA, Gerhart M, Davis R, Fitzner JN, Johnson RS, Paxton RJ, March CJ, Cerretti DP (1997) A metalloproteinase disintegrin that releases tumour-necrosis factor-alpha from cells. *Nature* **385:** 729–733

Blobel CP (2005) ADAMs: key components in EGFR signalling and development. *Nat Rev Mol Cell Biol* **6:** 32–43

Blobel CP, Myles DG, Primakoff P, White JM (1990) Proteolytic processing of a protein involved in sperm-egg fusion correlates with acquisition of fertilization competence. *J Cell Biol* **111:** 69–78

Blobel CP, Wolfsberg TG, Turck CW, Myles DG, Primakoff P, White JM (1992) A potential fusion peptide and an integrin ligand domain in a protein active in sperm-egg fusion. *Nature* **356:** 248–252

Bode W, Gomis-Ruth FX, Stockler W (1993) Astacins, serralysins, snake venom and matrix metalloproteinases exhibit identical zinc-binding environments (HEXXHXXGXXH and Met-turn) and

topologies and should be grouped into a common family, the 'metzincins'. *FEBS Lett* **331:** 134–140

Bridges LC, Hanson KR, Tani PH, Mather T, Bowditch RD (2003) Integrin alpha4beta1-dependent adhesion to ADAM 28 (MDC-L) requires an extended surface of the disintegrin domain. *Biochemistry* **42:** 3734–3741

Brunger AT, Adams PD, Clore GM, DeLano WL, Gros P, Grosse-Kunstleve RW, Jiang JS, Kuszewski J, Nilges M, Pannu NS, Read RJ, Rice LM, Simonson T, Warren GL (1998) Crystallography & NMR system: a new software suite for macromolecular structure determination. *Acta Crystallogr D* **54** (Part 5): 905–921

Calvete JJ, Marcinkiewicz C, Monleon D, Esteve V, Celda B, Juarez P, Sanz L (2005) Snake venom disintegrins: evolution of structure and function. *Toxicon* **45:** 1063–1074

CCP4 (1994) The CCP4 suite: programs for protein crystallography. *Acta Crystallogr D* **50:** 760–763

Duffy MJ, Lynn DJ, Lloyd AT, O'Shea CM (2003) The ADAMs family of proteins: from basic studies to potential clinical applications. *Thromb Haemost* **89:** 622–631

Eto K, Huet C, Tarui T, Kupriyanov S, Liu HZ, Puzon-McLaughlin W, Zhang XP, Sheppard D, Engvall E, Takada Y (2002) Functional classification of ADAMs based on a conserved motif for binding to integrin alpha 9beta 1: implications for sperm-egg binding and other cell interactions. *J Biol Chem* **277:** 17804–17810

Evans JP (2001) Fertilin beta and other ADAMs as integrin ligands: insights into cell adhesion and fertilization. *BioEssays* **23:** 628–639

Fox JW, Serrano SM (2005) Structural considerations of the snake venom metalloproteinases, key members of the M12 reprolysin family of metalloproteinases. *Toxicon* **45:** 969–985

Fujii Y, Okuda D, Fujimoto Z, Horii K, Morita T, Mizuno H (2003) Crystal structure of trimestatin, a disintegrin containing a cell adhesion recognition motif RGD. *J Mol Biol* **332:** 1115–1122

Gaultier A, Cousin H, Darribere T, Alfandari D (2002) ADAM13 disintegrin and cysteine-rich domains bind to the second heparin-binding domain of fibronectin. *J Biol Chem* **277:** 23336–23344

Huang TF, Holt JC, Lukasiewicz H, Niewiarowski S (1987) Trigramin. A low molecular weight peptide inhibiting fibrinogen interaction with platelet receptors expressed on glycoprotein IIb–IIIa complex. *J Biol Chem* **262:** 16157–16163

Iba K, Albrechtsen R, Gilpin B, Frohlich C, Loechel F, Zolkiewska A, Ishiguro K, Kojima T, Liu W, Langford JK, Sanderson RD, Brakebusch C, Fassler R, Wewer UM (2000) The cysteine-rich domain of human ADAM 12 supports cell adhesion through syndecans and triggers signaling events that lead to beta1 integrin-dependent cell spreading. *J Cell Biol* **149:** 1143–1156

Janes PW, Saha N, Barton WA, Kolev MV, Wimmer-Kleikamp SH, Nievergall E, Blobel CP, Himanen JP, Lackmann M, Nikolov DB (2005) Adam meets Eph: an ADAM substrate recognition module acts as a molecular SWITCH for Ephrin cleavage *in trans*. *Cell* **123:** 291–304

Jia LG, Shimokawa K, Bjarnason JB, Fox JW (1996) Snake venom metalloproteinases: structure, function and relationship to the ADAMs family of proteins. *Toxicon* **34:** 1269–1276

Jia LG, Wang XM, Shannon JD, Bjarnason JB, Fox JW (2000) Inhibition of platelet aggregation by the recombinant cysteine-rich domain of the hemorrhagic snake venom metalloproteinase, atrolysin A. *Arch Biochem Biophys* **373:** 281–286

Kamiguti AS, Gallagher P, Marcinkiewicz C, Theakston RD, Zuzel M, Fox JW (2003) Identification of sites in the cysteine-rich domain of the class P-III snake venom metalloproteinases responsible for inhibition of platelet function. *FEBS Lett* **549:** 129–134

Maskos K, Fernandez-Catalan C, Huber R, Bourenkov GP, Bartunik H, Ellestad GA, Reddy P, Wolfson MF, Rauch CT, Castner BJ, Davis R, Clarke HR, Petersen M, Fitzner JN, Cerretti DP, March CJ, Paxton RJ, Black RA, Bode W (1998) Crystal structure of the catalytic domain of human tumor necrosis factor-alpha-converting enzyme. *Proc Natl Acad Sci USA* **95:** 3408–3412

Masuda S, Hayashi H, Araki S (1998) Two vascular apoptosis-inducing proteins from snake venom are members of the metalloprotease/disintegrin family. *Eur J Biochem* **253:** 36–41

Masuda S, Ohta T, Kaji K, Fox JW, Hayashi H, Araki S (2000) cDNA cloning and characterization of vascular apoptosis-inducing protein 1. *Biochem Biophys Res Commun* **278:** 197–204

Moss ML, Bartsch JW (2004) Therapeutic benefits from targeting of ADAM family members. *Biochemistry* **43:** 7227–7235

Moss ML, Jin SL, Milla ME, Bickett DM, Burkhart W, Carter HL, Chen WJ, Clay WC, Didsbury JR, Hassler D, Hoffman CR, Kost TA, Lambert MH, Leesnitzer MA, McCauley P, McGeehan G, Mitchell J, Moyer M, Pahel G, Rocque W, Overton LK, Schoenen F, Seaton T, Su JL, Warner J, Willard D, Becherer JD (1997) Cloning of a disintegrin metalloproteinase that processes precursor tumour-necrosis factor-alpha. *Nature* **385:** 733–736

Myles DG, Kimmel LH, Blobel CP, White JM, Primakoff P (1994) Identification of a binding site in the disintegrin domain of fertilin required for sperm-egg fusion. *Proc Natl Acad Sci USA* **91:** 4195–4198

Nakamura T, Abe H, Hirata A, Shimoda C (2004) ADAM family protein Mde10 is essential for development of spore envelopes in the fission yeast *Schizosaccharomyces pombe*. *Eukaryot Cell* **3:** 27–39

Orth P, Reichert P, Wang W, Prosise WW, Yarosh-Tomaine T, Hammond G, Ingram RN, Xiao L, Mirza UA, Zou J, Strickland C, Taremi SS, Le HV, Madison V (2004) Crystal structure of the catalytic domain of human ADAM33. *J Mol Biol* **335:** 129–137

Pan D, Rubin GM (1997) Kuzbanian controls proteolytic processing of Notch and mediates lateral inhibition during *Drosophila* and vertebrate neurogenesis. *Cell* **90:** 271–280

Perrakis A, Morris R, Lamzin VS (1999) Automated protein model building combined with iterative structure refinement. *Nat Struct Biol* **6:** 458–463

Primakoff P, Hyatt H, Tredick-Kline J (1987) Identification and purification of a sperm surface protein with a potential role in sperm-egg membrane fusion. *J Cell Biol* **104:** 141–149

Qi H, Rand MD, Wu X, Sestan N, Wang W, Rakic P, Xu T, Artavanis-Tsakonas S (1999) Processing of the notch ligand delta by the metalloprotease Kuzbanian. *Science* **283:** 91–94

Reddy P, Slack JL, Davis R, Cerretti DP, Kozlosky CJ, Blanton RA, Shows D, Peschon JJ, Black RA (2000) Functional analysis of the domain structure of tumor necrosis factor-alpha converting enzyme. *J Biol Chem* **275:** 14608–14614

Rooke J, Pan D, Xu T, Rubin GM (1996) KUZ, a conserved metalloprotease-disintegrin protein with two roles in *Drosophila* neurogenesis. *Science* **273:** 1227–1231

Seals DF, Courtneidge SA (2003) The ADAMs family of metalloproteases: multidomain proteins with multiple functions. *Genes Dev* **17:** 7–30

Serrano SM, Jia LG, Wang D, Shannon JD, Fox JW (2005) Function of the cysteine-rich domain of the haemorrhagic metalloproteinase atrolysin A: targeting adhesion proteins collagen I and von Willebrand factor. *Biochem J* **391:** 69–76

Smith KM, Gaultier A, Cousin H, Alfandari D, White JM, DeSimone DW (2002) The cysteine-rich domain regulates ADAM protease function *in vivo*. *J Cell Biol* **159:** 893–902

Van Eerdewegh P, Little RD, Dupuis J, Del Mastro RG, Falls K, Simon J, Torrey D, Pandit S, McKenny J, Braunschweiger K, Walsh A, Liu Z, Hayward B, Folz C, Manning SP, Bawa A, Saracino L, Thackston M, Benchekroun Y, Capparell N, Wang M, Adair R, Feng Y, Dubois J, FitzGerald MG, Huang H, Gibson R, Allen KM, Pedan A, Danzig MR, Umland SP, Egan RW, Cuss FM, Rorke S, Clough JB, Holloway JW, Holgate ST, Keith TP (2002) Association of the ADAM33 gene with asthma and bronchial hyperresponsiveness. *Nature* **418:** 426–430

White JM (2003) ADAMs: modulators of cell–cell and cell–matrix interactions. *Curr Opin Cell Biol* **15:** 598–606

Yagami-Hiromasa T, Sato T, Kurisaki T, Kamijo K, Nabeshima Y, Fujisawa-Sehara A (1995) A metalloprotease-disintegrin participating in myoblast fusion. *Nature* **377:** 652–656

Zhu X, Teng M, Niu L (1999) Structure of acutolysin-C, a haemorrhagic toxin from the venom of Agkistrodon acutus, providing further evidence for the mechanism of the pH-dependent proteolytic reaction of zinc metalloproteinases. *Acta Crystallogr D* **55:** 1834–1841

Zolkiewska A (1999) Disintegrin-like/cysteine-rich region of ADAM 12 is an active cell adhesion domain. *Exp Cell Res* **252:** 423–431

Available online at www.sciencedirect.com
ScienceDirect
Neurochemistry International 49 (2006) 448–453
NEUROCHEMISTRY International
www.elsevier.com/locate/neuint

Effect of sustained limb ischemia on norepinephrine release from skeletal muscle sympathetic nerve endings

Yosuke Kuroko [a], Noriyuki Tokunaga [b], Toji Yamazaki [b,*], Tsuyoshi Akiyama [b], Kozo Ishino [a], Shunji Sano [a], Hidezo Mori [b]

[a] *Department of Cardiovascular Surgery, Okayama University Graduate School of Medicine and Dentistry, Okayama 700-8558, Japan*
[b] *Department of Cardiac Physiology, National Cardiovascular Center Research Institute, 5-7-1 Fujishiro-dai, Suita, Osaka 565-8565, Japan*

Received 8 October 2005; accepted 2 March 2006
Available online 24 April 2006

Abstract

Acute ischemia has been reported to impair sympathetic outflow distal to the ischemic area in various organs, whereas relatively little is known about this phenomenon in skeletal muscle. We examined how acute ischemia affects norepinephrine (NE) release at skeletal muscle sympathetic nerve endings. We implanted a dialysis probe into the adductor muscle in anesthetized rabbits and measured dialysate NE levels as an index of skeletal muscle interstitial NE levels. Regional ischemia was introduced by microsphere injection and ligation of the common iliac artery. The time courses of dialysate NE levels were examined during prolonged ischemia. Ischemia induced a decrease in the dialysate NE level (from 19 ± 4 to 2.0 ± 0 pg/ml, mean $\pm$ S.E.), and then a progressive increase in the dialysate NE level. The increment in the dialysate NE level was examined with local administration of desipramine (DMI, a membrane NE transport inhibitor), ω-conotoxin GVIA (CTX, an N-type Ca^{2+} channel blocker), or TMB-8 (an intracellular Ca^{2+} antagonist). At 4 h ischemia, the increment in the dialysate NE level (vehicle group, 143 ± 30 pg/ml) was suppressed by TMB-8 (25 ± 5 pg/ml) but not by DMI (128 ± 10 pg/ml) or CTX (122 ± 18 pg/ml). At 6 h ischemia, the increment in the dialysate NE level was not suppressed by the pretreatment. Ischemia induced biphasic responses in the skeletal muscle. Initial reduction of NE release may be mediated by an impairment of axonal conduction and/or NE release function, while in the later phase, the skeletal muscle ischemia-induced NE release was partly attributable to exocytosis via intracellular Ca^{2+} overload rather than opening of calcium channels or carrier mediated outward transport of NE.

Keywords: Catecholamine; Interstitial space; Microdialysis; Rabbit; Striate muscle

1. Introduction

Acute ischemia has been reported to be associated with impairment of the sympathetic tract (Schömig et al., 1984; Toyohara et al., 1986; Fujii et al., 2003). A well-known example is myocardial ischemia associated with impairment of the regional cardiac sympathetic nerve endings (Schömig et al., 1984; Ciuffo et al., 1985). Outward norepinephrine (NE) transport through uptake$_1$ carrier has been proposed as one of the main mechanisms responsible for ischemia-induced NE efflux from sympathetic nerve endings (Schömig et al., 1984; Akiyama and Yamazaki, 2001). However, little is known about the sympathetic impairment evoked by skeletal muscle ischemia. Histochemical and electrophysiological studies (Barker and Saito, 1981; Hill et al., 1996) have identified sympathetic innervation in skeletal muscle, which exerted actions on the regulation of regional blood flow and glucose metabolism (Thompson and Mohrman, 1983; Fagius and Berne, 1994). During and after exercise, muscle sympathetic nerve activity has been reported to be modulated by ischemia-induced metaboreceptor stimulation (Cornett et al., 2000; Cui et al., 2001). Furthermore, skeletal muscle may be exposed to prolonged severe ischemia (Welsh and Lindinger, 1993). Severe skeletal muscle ischemia occurs with trauma, vascular diseases, and compartment syndrome. It is so far unknown whether severe muscle ischemia induces excessive NE release from muscle sympathetic nerve endings.

In view of energy metabolism, cardiac ischemia is characterized by rapid deterioration of cardiac function, which has been linked to a fall in intracellular pH, increased levels of inorganic phosphate and reduction in free energy changes of ATP-hydrolysis (Mair, 1999). In contrast to cardiac muscle,

* Corresponding author. Tel.: +81 6 6833 5012; fax: +81 6 6872 8092.
E-mail address: yamazaki@ri.ncvc.go.jp (T. Yamazaki).

0197-0186/$ – see front matter © 2006 Elsevier Ltd. All rights reserved.
doi:10.1016/j.neuint.2006.03.004

energy requirements in skeletal muscle are dependent on exercise and are reduced in the resting state since only resting tone is maintained (Idström et al., 1990; Lindsay et al., 1990). Typically, prolonged skeletal muscle ischemia imposes a metabolic stress that results in a depletion of glycogen, high-energy phosphagen, and adenine nucleotides (Welsh and Lindinger, 1993). Thus, a differential time course of energy metabolism occurs in the skeletal muscle and cardiac myocardium. No studies have systematically characterized the impairment of sympathetic nerves in the skeletal muscle ischemia.

Recently, we reported that microdialysis technique with high-performance liquid chromatography is a sensitive and versatile method for monitoring interstitial NE concentrations in myocardial ischemic regions (Akiyama et al., 1991, 1993). Moreover, we applied microdialysis technique to skeletal muscle and have reported that skeletal muscle dialysate NE serves as an index of muscle sympathetic nerve activity (Tokunaga et al., 2003a). Using this method, we investigated how acute skeletal muscle ischemia affects NE release from skeletal muscle sympathetic nerve endings and the mechanism of skeletal muscle ischemia-induced NE release with regional pharmacological intervention.

2. Methods

2.1. Animal model

The investigation conformed with the *Guide for the Care and Use of Laboratory Animals* published by the US National Institutes of Health (NIH Publication No. 85-23, revised 1996). Forty-two male Japanese white rabbits weighing 2.2–3.8 kg were used for the model of skeletal muscle ischemia. The animals were anesthetized with pentobarbital sodium (30–35 mg/kg) and ventilated with room air mixed with oxygen. The level of anesthesia was maintained with a continuous intravenous infusion of pentobarbital sodium (1–2 mg/kg/h). Body temperature was maintained with a heated pad and lamp. An electrocardiogram, heart rate (HR), and mean arterial blood pressure (MAP) were simultaneously monitored with a data recorder. After a longitudinal skin incision was made in the left groin, the dialysis probes were implanted in the left adductor muscle with a fine guiding needle.

2.2. Dialysis technique and NE measurements

With the dialysis technique, dialysate NE levels were measured as an index of skeletal muscle interstitial NE levels. For skeletal muscle dialysis, we designed a transverse dialysis probe. The dialysis fiber (13 mm length, 0.31 mm o.d. and 0.2 mm i.d.; PAN-1200, 50,000 molecular mass cut-off, Asahi Chemical, Tokyo, Japan) was glued at both ends into a polyethylene tube (25 cm length, 0.5 mm o.d. and 0.2 mm i.d.) (Akiyama et al., 1991). The dialysis probe was perfused with Ringer solution using a microinjection pump (CMA 102, Carnegie Medicin, Stockholm, Sweden). Similar to previous studies (Tokunaga et al., 2003a, 2003b), we chose a perfusion speed of 10 μl/min for skeletal muscle. Sampling periods were set at 15 min for skeletal muscle. Dialysate NE levels were measured by high-performance liquid chromatography with electrochemical detection (ECD-300, Eicom, Kyoto, Japan) after removing interfering compounds in the dialysate by an alumina procedure (Anton and Sayer, 1962; Akiyama et al., 1991). Dialysate dihydroxyphenylglycol (DHPG) levels were measured by separate high-performance liquid chromatography with electrochemical detection (Akiyama and Yamazaki, 2001).

2.3. Experimental protocols

Acute skeletal muscle ischemia was induced by injection of non-radioactive iodine-labeled microspheres (15 μm in diameter, 3×10^7/kg, Sekisui Plastic, Osaka, Japan) through the left common iliac artery, as previously described (Tanaka et al., 2000). After the injection of microspheres, the common iliac artery was ligated.

2.3.1. Protocol 1: time courses of dialysate NE levels during acute ischemia

To examine the time courses of dialysate NE levels during acute skeletal muscle ischemia, we measured dialysate NE levels over 60-min periods of skeletal muscle ischemia ($n = 6$). We collected four consecutive 15-min dialysate samples. Furthermore, we measured dialysate NE samples over a period of 6 h of skeletal muscle ischemia with 2 h interval in separate rabbits. To examine intraneuronal NE kinetics in the skeletal muscle, the measurement of dialysate DHPG level was added during 6 h of skeletal muscle ischemia ($n = 6$).

2.3.2. Protocol 2: involvement of NE uptake$_1$ transport, Ca^{2+} channels and cytosol Ca^{2+} in dialysate NE levels during acute ischemia

To examine the mechanism underlying the increment of NE release during the prolonged ischemia, dialysate NE levels were measured with regional pharmacological intervention. Neurotransmitter release from sympathetic nerve endings can be caused by a variety of different mechanisms (Schömig et al., 1987; Kawada et al., 2000; Akiyama and Yamazaki, 2001). In the present studies, we examined the roles of membrane NE transport, N-type Ca^{2+} channels and cytosol Ca^{2+} in the time courses of dialysate NE levels during prolonged ischemia. To examine the involvement of membrane NE transport in the ischemia-induced NE release, we locally administered an uptake$_1$ carrier blocker, desipramine (100 μM) through a dialysis probe and observed the responses of dialysate NE (Akiyama and Yamazaki, 2001) ($n = 6$). The same protocol was performed with addition of a voltage-dependent N-type Ca^{2+} channel blocker, ω-conotoxin GVIA (10 μM) ($n = 6$) or intracellular Ca^{2+} antagonist, 8-(*N*,*N*-diethylamino)-octyl-3,4,5-trimethoxybenzoate hydrochloride (TMB-8, 1 mM) ($n = 6$) through a dialysis probe. From data on protocol 1, we observed increases in dialysate NE levels after 2 h of skeletal muscle ischemia. Therefore, the time course of dialysate NE for skeletal muscle ischemia was examined over a period of 6 h with a 2 h-interval ($n = 6$). The effectiveness of ω-conotoxin GVIA (10 μM) ($n = 6$) or TMB-8 (1 mM) ($n = 6$) was tested before the experiment in separate rabbits. We administered high potassium (KCl, 100 mM) locally through the dialysis probe, and the dialysate NE response was obtained in the presence and absence of ω-conotoxin GVIA or TMB-8. High-K increased dialysate NE from 11.7 ± 2.8 to 84.7 ± 20.8 pg/ml ($n = 6$). This KCl-induced increment in dialysate NE was attenuated by the addition of ω-conotoxin GVIA or TMB-8 (Fig. 1).

2.3.3. Protocol 3: time courses of dialysate lactate levels during the hind limb ischemia

To confirm whether this perturbation induces tissue ischemia, we examined the time course of dialysate lactate levels as an index of tissue ischemia. The dialysate lactate levels were measured by kinetic enzymatic analysis with CMA 600 (Carnegie Medicin). In the skeletal muscle ischemia, four consecutive 15-

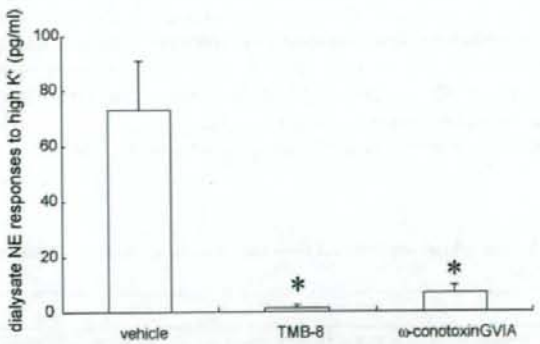

Fig. 1. Effects of pharmacological intervention on dialysate norepinephrine (NE) responses to high K^+ (KCl, 100 mM). Both TMB-8 (1 mM) and ω-conotoxin (10 μM) suppressed dialysate responses to high K^+. Values are means ± S.E. ($n = 6$).

min dialysate samples were collected during the initial 60-min and subsequently three consecutive samples were collected over a period of 6 h with a 2 h-interval ($n = 6$).

2.4. Statistical analysis

All data are presented as mean ± S.E. values. Hemodynamic and dialysate data responses to acute ischemia were statistically analyzed by analysis of variance with repeated measures. When a statistically significant effect of ischemia was detected as a whole, the Dunnett's test was applied to determine which mean values differed significantly from the control level. When a statistically significant effect of the treatment was detected, Newman–Keuls test was applied to determine which treatment differed significantly from the vehicle.

3. Results

Table 1 summarizes changes in HR and MAP. MAP and HR increased during 6 h-hind limb ischemia. Changes in MAP at 2 h and HR at 6 h-hind limb ischemia were significant.

3.1. Time courses of dialysate NE levels during short and prolonged ischemia

Skeletal muscle dialysate NE levels decreased from 19 ± 4 pg/ml at control to 9 ± 4 pg/ml at 30 min of ischemia and reached 2 ± 0 pg/ml at 60 min of ischemia (Fig. 2). The decrease in dialysate NE level was maintained after 2 h of ischemia. Then skeletal muscle dialysate NE levels markedly increased to 143 ± 30 pg/ml at 4 h of ischemia. The dialysate NE levels continued to increase progressively and reached 289 ± 45 pg/ml at 6 h of ischemia. Skeletal muscle dialysate DHPG levels decreased from 38 ± 2 pg/ml at control to 5 ± 1 pg/ml at 2 h of ischemia and reached 7 ± 1 pg/ml at 6 h of ischemia.

3.2. Involvement of NE uptake$_1$ transport, Ca^{2+} channels and cytosol Ca^{2+} in dialysate NE levels during prolonged ischemia

Dialysate NE increases at 4 and 6 h-skeletal muscle ischemia were not suppressed by treatment with desipramine (Fig. 3). Dialysate NE increases at 4 and 6 h-skeletal muscle ischemia were not suppressed by treatment with ω-conotoxin GVIA. Treatment with TMB-8 significantly suppressed the dialysate NE increase at 4 h-skeletal muscle ischemia. But at 6 h-skeletal muscle ischemia, there was no significant difference in dialysate NE levels among treatments.

Table 1
Changes in heart rate (HR) and mean arterial pressure (MAP) in 6 h-hindlimb ischemia

	Control	2 h	4 h	6 h
HR (beats/min)	283 ± 10	292 ± 4	293 ± 8	302 ± 8*
MAP (mmHg)	104 ± 6	114 ± 3*	111 ± 4	108 ± 4

Values are means ± S.E. from six rabbits. Data were obtained during control, after 2, 4, and 6 h of hind limb ischemia.
* $P < 0.05$ vs. control.

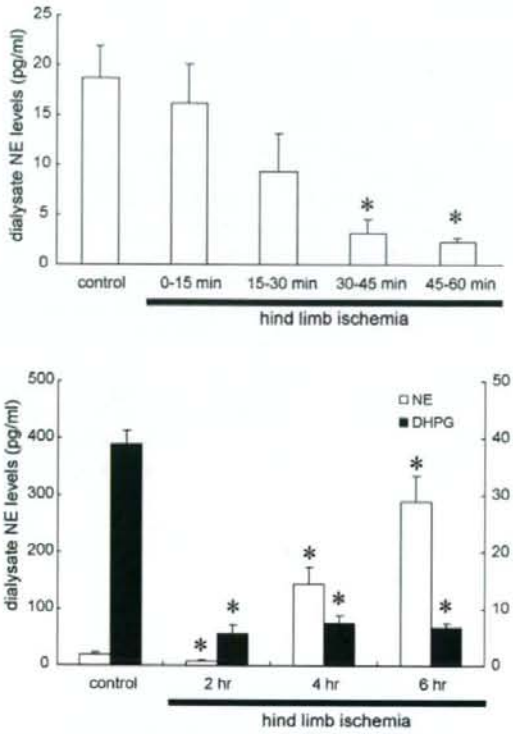

Fig. 2. (Upper panel) Time course of dialysate norepinephrine (NE) levels during 60 min-hind limb ischemia. Values are means ± S.E. ($n = 6$). *$P < 0.05$ vs. control value. (Lower panel) Time courses of dialysate NE and dihydroxyphenylglycol (DHPG) levels during 6 h-hind limb ischemia. Values are means ± S.E. ($n = 6$). *$P < 0.05$ vs. control value.

3.3. Time course of dialysate lactate levels during hind limb ischemia

Skeletal muscle dialysate lactate levels increased from 0.6 ± 0.07 nmol/l at control to 1.73 ± 0.17 nmol/l at 45–60 min

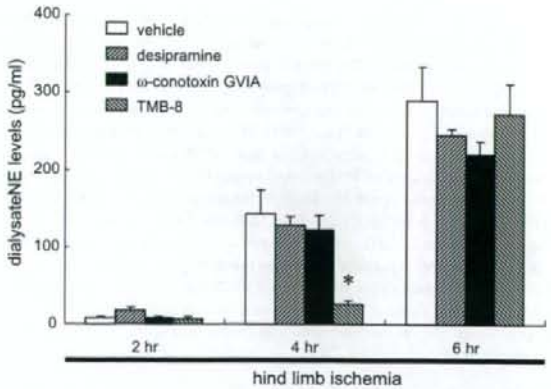

Fig. 3. Effects of pharmacological intervention on dialysate norepinephrine (NE) levels evoked by 6 h-hind limb ischemia. Desipramine (100 μM), ω-conotoxin (10 μM), or TMB-8 (1mM) was locally administered through the probe. Values are means ± S.E. ($n = 6$). *$P < 0.05$ vs. concurrent value of vehicle group.

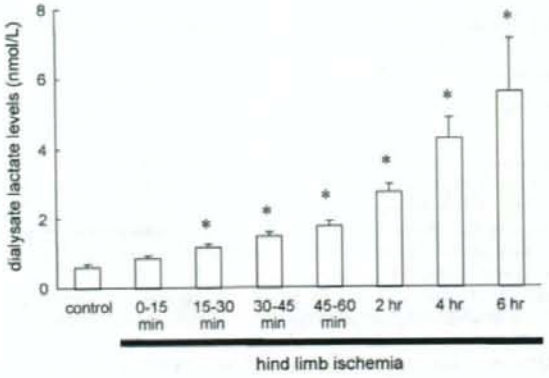

Fig. 4. Time course of dialysate lactate levels during 6 h-hind limb ischemia. Values are means ± S.E. ($n = 6$). $^{*}P < 0.05$ vs. control value.

of ischemia (Fig. 4). These step-wise increases were continued for 6 h of the hind limb ischemia.

4. Discussion

Using dialysis techniques in the in vivo rabbit skeletal muscle, we examined interstitial levels of NE in the control and ischemic period, and observed the biphasic response of dialysate NE in ischemic skeletal muscle. Ischemia induced an initial reduction followed by a progressive increment in dialysate NE levels. Here we discuss changes in interstitial NE and possible mechanisms underlying sympathetic nerve impairment.

Within 2 h of acute skeletal muscle ischemia, unlike acute myocardial ischemia, skeletal muscle interstitial NE levels continued to decline progressively, decreasing to one-tenth of control at 60 min of ischemia. A previous study demonstrated that skeletal muscle ischemia modulated the baroreflex control of regional muscle sympathetic activity (Cornett et al., 2000). At 75 min of acute skeletal muscle ischemia, hemodynamic responses to carotid occlusion were preserved while the interstitial NE response to carotid occlusion was blunted in the ischemic region (Tokunaga et al., 2003b). These results indicate that the systemic response to baroreflex remained intact while the skeletal muscle sympathetic response was impaired in ischemic regions. Earlier studies reported that acute limb ischemia reduced the conduction of motor nerves such as sciatic nerve (Fern and Harrison, 1994), and induced axonal degeneration histologically (Makitie and Teravainen, 1977; Nukada and Dyek, 1987). Axonal conduction in the ischemic muscle sympathetic nerve may be impaired as well as in sensory and motor nerves. In addition to diminished axonal conductance, the interstitial NE response to high K^+ but not tyramine was suppressed during the 75 min of acute skeletal muscle ischemia, although NE content at muscle sympathetic nerve endings was preserved during the ischemia (Tokunaga et al., 2003b). This result indicates that exocytotic NE releasing function in muscle sympathetic nerve endings might be suppressed during 75 min of acute skeletal muscle ischemia. Therefore, initial reduction of NE release may be mediated by an impairment of axonal conduction and/or NE releasing function.

After 2 h of acute skeletal muscle ischemia, skeletal muscle interstitial NE levels significantly increased and finally reached 20-fold that of control. This amount of NE release is higher than that evoked by baroreflex or high K^+. This level is similar to that evoked by the Na^+–K^+ ATPase inhibitor, ouabain (Tokunaga et al., 2003a). The amount of NE release evoked by ischemia may be dependent on the density of sympathetic innervation. Dispersed organ systems such as skeletal muscle have a thin and diffuse sympathetic innervation. This is the first report to describe that marked NE release is induced from muscle sympathetic nerve endings in the ischemic region after 2 h of skeletal muscle ischemia. Numerous histological changes of skeletal muscle have been reported after ischemia and reperfusion injury (Patterson and Klenerman, 1979; Turchányi et al., 2005). However, there is no histochemical evidence of the impaired sympathetic nerves in the skeletal muscle ischemia.

In the case of skeletal muscle ischemia, ω-conotoxin GVIA did not suppress NE efflux. N-type Ca^{2+} channels are not involved in this NE efflux. Desipramine did not alter NE efflux during skeletal muscle ischemia. Desipramine inhibits carrier-mediated NE transport in both directions. Considering that desipramine did not alter interstitial NE levels, the amounts of NE release and uptake via normal transport can be surmised to be negligible. Second, the increase in skeletal muscle interstitial NE levels was not associated with an increase in skeletal muscle interstitial DHPG levels, indicating that skeletal ischemia fails to induce axoplasmic NE elevation via alterations in monoamine activity, NE mobilization from stored vesicle, and NE uptake. Further, desipramine did not suppress NE efflux. These results exclude the possibility that marked increases in skeletal muscle interstitial NE could be due to carrier-mediated outward transport of NE for removal of elevated axoplasmic NE concentration. The membrane NE transporter exists in the skeletal muscle sympathetic nerve endings (Cabassi et al., 2001; Tokunaga et al., 2003a), but was not involved in outward transport of NE. Thus, we consider that a ω-conotoxin GVIA insensitive and desipramine-resistant NE release mechanism exists after 2 h of acute skeletal muscle ischemia.

TMB-8 significantly suppressed the marked NE release at 4 h of skeletal muscle ischemia. TMB-8 is well known to inhibit Ca^{2+} release from intracellular Ca^{2+} stores. TMB-8 inhibits caffeine-induced catecholamine release from perfused adrenal gland in the absence of extracellular Ca^{2+} (Yamada et al., 1988). Studies using chromaffin cells, brain slices and synaptosomes have suggested that metabolic inhibition induces intracellular Ca^{2+} overload (Milusheva et al., 1992), and a rise in the intracellular Ca^{2+} causes exocytotic catecholamine release without membrane depolarization (Dry et al., 1991; Du et al., 1997). Moreover, an in vitro study with adrenergic nerves of guinea-pig vas deferens suggested that Ca^{2+} release from intracellular Ca^{2+} stores is to some extent involved in the NE release evoked by elevation of intracellular Na^+ (Katsuragi et al., 1994). Under energy-depleted conditions, Ca^{2+} overload

in synaptosomes of noradrenergic neurons from the brain is an important mechanism for the enhanced release of neurotransmitter, with a reversal of Na^+–Ca^{2+} exchange possibly the key pathway leading to intraneuronal Ca^{2+} overload (Du et al., 1997). We consider that Ca^{2+} release from intracellular Ca^{2+} stores is partly involved in the NE release at 4 h of skeletal muscle ischemia.

At 6 h of skeletal ischemia, increment in dialysate NE level was not suppressed by the pretreatments. This result suggests that another mechanism may be involved in NE release, which is insensitive to desipramine, ω-conotoxin GVIA, and TMB-8. Alternatively, the NE release may occur with development of irreversible membrane damage and can no longer be inhibited by pharmacological interventions. Future work should concentrate on these aspects of NE release during the later period.

4.1. Methodological considerations

The limitation of this experiment is related to the methodology and the duration of the hind limb ischemia. In a variety of these experimental models for organ ischemia, we chose microsphere injection and iliac artery occlusion for the short and prolonged hind limb ischemia model. A preliminary experiment indicated that common iliac artery occlusion did not yield severe ischemia or muscle necrosis in a chronic ischemic model because collateral flow prevents skeletal muscle ischemia. The combination of artery occlusion and injection of microsphere was used for the hind limb ischemic model. In the hind limb ischemia, however, we did not measure skeletal muscle blood flow. To confirm whether this perturbation induced reduction of blood flow and tissue ischemia, we measured dialysate lactate levels in skeletal muscle as an index of tissue ischemia. This perturbation induced increases in dialysate lactate levels. In the present study, dialysate NE responses were examined in prolonged 6 h ischemia. Temporal changes in MAP and HR appeared but sustained significant hemodynamic changes were not observed. This duration was referred to the experiments on the tourniquet application and release time (Sapega et al., 1985; Mitrev et al., 1996). Four to 6 h of ischemic periods has been thought to produce extensive and reversible damage of skeletal muscle. Therefore, data on pharmacological intervention were obtained within 6 h of skeletal muscle ischemia.

Ischemia induced biphasic NE responses in the skeletal muscle. Initial reduction of NE release may be mediated by an impairment of axonal conduction and/or NE releasing function, while in the later phase, the skeletal muscle ischemia-induced NE release was partly attributable to exocytosis via intracellular Ca^{2+} overload rather than opening of calcium channels or carrier mediated outward transport of NE.

Acknowledgements

This study was supported by Grants-in Aid for scientific research (15590787) from the Ministry of Education, Culture, Sports, Science and Technology; the Research Grants for Cardiovascular Disease (H13C-1) from the Ministry of Health, Labor and Welfare.

References

Akiyama, T., Yamazaki, T., Ninomiya, I., 1991. In vivo monitoring of myocardial interstitial norepinephrine by dialysis technique. Am. J. Physiol. 261, H1643–H1647.

Akiyama, T., Yamazaki, T., Ninomiya, I., 1993. Differential regional responses of myocardial interstitial noradrenaline levels to coronary occlusion. Cardiovasc. Res. 27, 817–822.

Akiyama, T., Yamazaki, T., 2001. Myocardial interstitial norepinephrine and dihydroxyphenylglycol levels during ischemia and reperfusion. Cardiovasc. Res. 49, 78–85.

Anton, A.H., Sayer, D.F., 1962. A study of the factors affecting the aluminum oxide-trihydroxyindole procedure for the analysis of catecholamine. J. Pharmacol. Exp. Ther. 138, 360–375.

Barker, D., Saito, M., 1981. Autonomic innervation of receptors and muscle fibers in cat skeletal muscle. Proc. Roy. Soc. Lond., B: Biol. Sci. 212, 317–332.

Cabassi, A., Vinci, S., Quartieri, F., Moschini, L., Borghetti, A., 2001. Norepinephrine uptake is impaired in skeletal muscle of hypertensive rats in vivo. Hypertension 37, 698–702.

Ciuffo, A.A., Ouyang, P., Becker, L.C., Levin, L., Weisfeldt, M.L., 1985. Reduction of sympathetic inotropic response after ischemia in dogs. Contributor to stunned myocardium. J. Clin. Invest. 75, 1504–1509.

Cornett, J.A., Herr, M.D., Gray, K.S., Smith, M.B., Yang, Q.X., Sinoway, L.I., 2000. Ischemic exercise and the muscle metaboreflex. J. Appl. Physiol. 89, 1432–1436.

Cui, J., Wilson, T.E., Shibasaki, M., Hodges, N.A., Grandall, C.G., 2001. Baroreflex modulation of muscle sympathetic nerve activity during postgrip muscle ischemia in human. J. Appl. Physiol. 91, 1679–1686.

Dry, K.L., Phillips, J.H., Dart, A.M., 1991. Catecholamine release from bovine adrenal chromaffin cells during anoxia or metabolic inhibition. Circ. Res. 69, 466–474.

Du, X.-J., Bobik, A., Little, P.J., Esler, M.D., Dart, A.M., 1997. Role of Ca^{2+} in metabolic inhibition-induced norepinephrine release in rat brain synaptosomes. Circ. Res. 80, 179–188.

Fagius, J., Berne, C., 1994. Increase in muscle sympathetic activity in humans after food intake. Clin. Sci. (London) 86, 159–167.

Fern, R., Harrison, P.J., 1994. The relationship between ischaemic conduction failure and conduction velocity in cat myelinated axons. Exp. Physiol. 79, 571–581.

Fujii, T., Kurata, H., Takaoka, M., Muraoka, T., Fujisawa, Y., Shokoji, T., Nishiyama, A., Abe, Y., Matsumura, Y., 2003. The role of renal sympathetic nervous system in the pathogenesis of ischemic acute renal failure. Eur. J. Pharmacol. 481, 241–248.

Hill, J.M., Adreani, C.M., Kaufman, M.P., 1996. Muscle reflex stimulates sympathetic postganglionic efferents innervating triceps surae muscle of cats. Am. J. Physiol. 271, H38–H43.

Idström, J.-P., Soussi, B., Elander, A., Bylund-Fellenius, A.-C., 1990. Purine metabolism after in vivo ischemia and reperfusion in rat skeletal muscle. Am. J. Physiol. 258, H1668–H1673.

Katsuragi, T., Ogawa, S., Furukawa, T., 1994. Contribution of intra- and extracellular Ca^{2+} to noradrenaline exocytosis induced by ouabain and monensin from guinea-pig vas deferens. Br. J. Pharmacol. 113, 795–800.

Kawada, T., Yamazaki, T., Akiyama, T., Sato, T., Shishido, T., Inagaki, M., Tetewaki, T., Yanagiya, Y., Sugimachi, M., Sunagawa, K., 2000. Cyanide intoxication induced exocytotic epinephrine release in rabbit myocardium. J. Auton. Nerv. Syst. 80, 137–141.

Lindsay, T.F., Liauw, S., Romaschin, A.D., Walker, P.M., 1990. The effect of ischemia/reperfusion on adenine nucleotide metabolism and xanthine oxidase production in skeletal muscle. J. Vasc. Surg. 12, 8–15.

Mair, J., 1999. Tissue release of cardiac markers: from physiology to clinical applications. Clin. Chem. Lab. Med. 37, 1077–1084.

Makitie, J., Teravainen, H., 1977. Peripheral nerve injury and recovery after temporary ischemia. Acta Neuropathol. (Berl.) 37, 55–63.

Milusheva, E., Doda, M., Pasztor, E., Lajtha, A., Sershen, H., Vizi, E.S., 1992. Regulatory interactions among axonal terminals affecting the release of different transmitters from rat striatal slices under hypoxic and hypoglycemic conditions. J. Neurochem. 59, 946–952.

Mitrev, Z., Ihnken, K., Poloczek, Y., Hallmann, R., Herold, H., Unkelbach, U., Zimmer, G., Freisleben, H.J., Beyersdorf, S., Beyersdorf, F., 1996. Controlled reperfusion of the extremities for preventing local and systemic damage after prolonged ischemia. An experimental study with the swine model. Zentralbl. Chir. 121, 774–787.

Nukada, H., Dyck, P.J., 1987. Acute ischemia causes axonal stasis, swelling, attenuation and secondary demyelination. Ann. Neurol. 22, 311–318.

Patterson, S., Klenerman, 1979. The effect of pneumatic tourniquets on the ultrastructure of skeletal muscle. J. Bone Joint Surg. Br. 61, 178–183.

Schömig, A., Dart, A.M., Dietz, R., Mayer, E., Kubler, W., 1984. Release of endogenous catecholamines in the ischemic myocardium of the rat. Part A. Locally mediated release. Circ. Res. 55, 689–701.

Schömig, A., Fischer, S., Kurz, T., Richardt, G., Schömig, E., 1987. Non-exocytotic release of endogenous noradrenaline in the ischemic and anoxic rat heart: mechanism and metabolic requirements. Circ. Res. 60, 194–205.

Sapega, A.A., Heppenstall, R.B., Chance, B., Park, Y.S., Sokolow, D., 1985. Optimizing tourniquet application and release times in extremity surgery. A biochemical and ultrastructual study. J. Bone Joint Surg. Am. 67, 303–314.

Tanaka, E., Hattan, N., Ando, K., Ueno, H., Sugio, Y., Mohammed, M.U., Voltchikhina, S.A., Mori, H., 2000. Amelioration of microvascular myocardial ischemia by gene transfer of vascular endothelial growth factor in rabbits. J. Thorac. Cardiovasc. Surg. 120, 720–728.

Thompson, L.P., Mohrman, D.E., 1983. Blood flow and oxygen consumption in skeletal muscle during sympathetic stimulation. Am. J. Physiol. 245, H66–H71.

Tokunaga, N., Yamazaki, T., Akiyama, T., Sano, S., Mori, H., 2003a. In vivo monitoring of norepinephrine and its metabolites in skeletal muscle. Neurochem. Int. 43, 573–580.

Tokunaga, N., Yamazaki, T., Akiyama, T., Sano, S., Mori, H., 2003b. Acute limb ischemia does not facilitate but inhibits norepinephrine release from sympathetic nerve endings in anesthetized rabbit. J. Cardiovasc. Pharmacol. 42, S7–S10.

Toyohara, T., Nada, O., Ikeda, K., 1986. Influence of ischemia on noradrenergic nerves in the terminal colon of humans and rats. Eur. Surg. Res. 18, 349–355.

Turchányi, B., Tóth, B., Rácz, I., Vendégh, Z., Fűrész, J., Hamar, J., 2005. Ischemia reperfusion injury of the skeletal muscle after selective deafferentation. Physiol. Res. 54, 25–31.

Welsh, D.G., Lindinger, M.I., 1993. Energy metabolism and adenine nucleotide degradation in twitch-stimulated rat hindlimb during ischemia-reperfusion. Am. J. Physiol. 264, E655–E661.

Yamada, Y., Teraoka, H., Nakazato, Y., Ohga, A., 1988. Intracellular Ca^{2+} antagonist TMB-8 blocks catecholamine secretion evoked by caffeine and acetylcholine from perfused cat adrenal glands in the absence of extracellular Ca^{2+}. Neurosci. Lett. 90, 338–342.

WILEY InterScience® DISCOVER SOMETHING GREAT

Journal of Neuroscience Research 84:1187–1196 (2006)

Bcl2 Enhances Survival of Newborn Neurons in the Normal and Ischemic Hippocampus

Tsutomu Sasaki,[1]* Kazuo Kitagawa,[1] Yoshiki Yagita,[1] Shiro Sugiura,[1] Emi Omura-Matsuoka,[1] Shigeru Tanaka,[1] Kohji Matsushita,[1] Hideyuki Okano,[3] Yoshihide Tsujimoto,[2] and Masatsugu Hori[1]

[1]Division of Stroke Research, Department of Cardiovascular Medicine, Osaka University Graduate School of Medicine, Osaka, Japan
[2]Division of Molecular Genetics, Department of Post-Genomics and Diseases, Osaka University Graduate School of Medicine, Osaka, Japan
[3]Department of Physiology, Keio University Graduate School of Medicine, Shinjyuku-ku, Tokyo, Japan

Neuronal progenitors in the adult hippocampus continually proliferate and differentiate to the neuronal lineage, and ischemic insult promotes hippocampal neurogenesis. However, newborn neurons show a progressive reduction in numbers during the initial few weeks, therefore, enhanced survival of newborn neurons seems to be essential for therapeutic strategy. Bcl-2 is a crucial regulator of programmed cell death in CNS development and in apoptotic and necrotic cell death. Therefore, we tested whether Bcl-2 overexpression enhances survival of newborn neurons in the adult mouse hippocampus under normal and ischemic conditions. Many newborn neurons in the hippocampal dentate gyrus undergo apoptosis. Human Bcl-2 expression in NSE-bcl-2 transgenic mice began at the immature neuronal stage and remained constant in surviving mature neurons. Bcl-2 significantly increased survival of newborn neurons under both conditions, but particularly after ischemia, with decreased cell death of newborn neurons in NSE-bcl-2 transgenic mice. We also clarified the effect by Bcl-2 overexpression of enhanced survival of newborn neurons in primary hippocampal cultures with BrdU labeling. These findings suggest that Bcl-2 plays a crucial role in adult hippocampal neurogenesis under normal and ischemic conditions.

Key words: Bcl-2; hippocampus; neurogenesis; ischemia

In adult hippocampal neurogenesis, nascent neurons show a progressive reduction (Kempermann et al., 2003), and surviving neurons became integrated into the dentate granule cell circuitry (van Praag et al., 2002). Continued production of hippocampal granule cells is combined with elimination of cells via spontaneous apoptosis, with turnover occurring throughout life (Gould and Cameron, 1996; Young et al., 1999). Running exercise and enriched environment promote the survival of newborn neurons (van Praag et al., 1999; Young et al., 1999). Thus, enhanced survival of newborn neurons seems beneficial.

Brain ischemia enhances neurogenesis in the hippocampus (Liu et al., 1998; Yagita et al., 2001) and also induces migration of neuroblasts into lesions in nonneurogenic areas such as the striatum (Arvidsson et al., 2002). However, only a small fraction of these newborn neurons survive (Liu et al., 1998; Yagita et al., 2001; Arvidsson et al., 2002). Despite accumulating data on the mechanisms responsible for neuronal progenitor proliferation after ischemia, little is understood regarding the signals that control survival of newborn neuron after ischemia. Bcl-2 levels were increased in the hippocampus after ischemia (Chen et al., 1997). Bcl-2 has been shown to be protective against apoptotic and necrotic cell death in response to various stimuli, including exposure to glutamate or ischemia (Martinou et al., 1994; Adams and Cory, 1998; Kitagawa et al., 1998). Moreover, neurotrophins play a crucial role in adult neurogenesis following ischemia as well as under normal conditions (Pencea et al., 2001). Bcl-2 has been reported to mediate the survival effects of neurotrophins such as BDNF and NGF. Based on these findings, it is essential to examine the effect of Bcl-2 on the survival of newborn neurons after ischemia.

During central nervous system (CNS) development, BCL-2 has been shown to be a key regulator of programmed cell death (Abe-Dohmae et al., 1993; Martinou et al., 1994). Programmed cell death has often been found in regions in which neurogenesis persists throughout adulthood, including the hippocampus and olfactory bulb.

Contract grant sponsor: Japan Society for the Promotion of Science; Contract grant sponsor: Takeda Science Foundation.

*Correspondence to: Tsutomu Sasaki, Division of Stroke Research, Department of Cardiovascular Medicine, Osaka University Graduate School of Medicine, 2-2 Yamadaoka, Suita City, Osaka 565-0871, Japan. E-mail: sasaki@medone.med.osaka-u.ac.jp

Received 3 April 2006; Revised 29 June 2006; Accepted 30 June 2006

Published online 29 August 2006 in Wiley InterScience (www.interscience.wiley.com). DOI: 10.1002/jnr.21036

We sought to determine whether overexpression of the human *bcl-2* transgene increases survival of newborn neurons in the hippocampal dentate gyrus under normal and ischemic conditions.

MATERIALS AND METHODS

Animals

All research was conducted according to a protocol approved by the Institutional Animal Care and Use Committee of Osaka University Graduate School of Medicine. Adult 11- to 12-weeks-old male C57Black/6 mice and transgenic mice overexpressing BCL-2 under a neuron-specific enolase promoter (NSE-*bcl-2* transgenic mice) (Martinou et al., 1994) were used. NSE-*bcl-2* transgenic mice were backcrossed to C57Black/6 mice 10 times. The genotype was confirmed postmortem by PCR amplification of tail genomic DNA. The amount of Bcl-2 expression in wild-type and NSE-*bcl-2* transgenic mice were evaluated by Western blotting.

Bromodeoxyuridine Labeling Protocols and Immunohistochemistry

To quantify and evaluate the phenotype of newborn cells, bromodeoxyuridine (BrdU; Roche Diagnostics, Indianapolis, IN) was given four times every 2 hr during a period of 6 hr. At 1, 7, 14, 21, and 30 days after BrdU administration, mice were sacrificed under deep pentobarbital anesthesia and transcardially perfused with 4% paraformaldehyde (PFA). Brains were removed and fixed in 4% PFA at 4°C.

Next, we used NSE-*bcl-2* transgenic mice including wild-type mice. BrdU-labeling protocols and the processing were the same above. To examine the proliferation of newborn neurons in the SGZ in both groups, mice were sacrificed 1 day after BrdU administration. To evaluate the survival or differentiation of newborn neurons, mice were decapitated 30 days after BrdU administration.

Each tissue block was embedded in paraffins. The protocol of BrdU immunohistochemistry was described previously (Sasaki et al., 2003). Sections were treated in 50% formamide and 2× SSC and then incubated in 2N HCl. Sections were incubated with a rat monoclonal anti-BrdU antibody, 1 : 100 (Harlan Sera-Labo, Loughborough, UK) at 4°C overnight. Sections were then incubated with a biotinylated secondary antibody, and further incubated with a streptavidin–biotin–peroxidase complex (Vector Laboratories, Burlingame, CA). To count BrdU-positive cells, five sections from the hippocampus were cut every 120 μm beginning 1.4 mm caudal and 1.9 mm caudal to the bregma. In the hippocampus, the granular cell layer (GCL) and SGZ, defined as a zone two cell bodies wide along the border of the GCL and hilus, were considered together for quantification. The mean density of BrdU-positive cells in each mouse was calculated as the number of labeled nuclei divided by the area.

For double-immunofluorescence, 40 μm-thick free-floating sections were incubated with primary antibody at 4°C overnight. The following primary antibodies were used: a monoclonal antibody against human BCL-2 (Dakocytomation, Denmark A/S), a rat monoclonal anti-BrdU antibody, 1 : 100 (Harlan Sera-Labo, Loughborough, UK), mouse monoclonal anti-BrdU antibody, 1 : 200 (Amersham, Piscataway, NJ), mouse monoclonal anti-NeuN antibody, 1:200 (Chemicon, Temecula, CA), rabbit polyclonal anti-glial fibrillary acidic protein (GFAP) antibody, 1 : 200 (Sigma), goat polyclonal anti-double cortin (DCX) antibody, 1 : 100 (Santa Cruz Biotechnology, Santa Cruz, CA), rat monoclonal anti-Musashi-1 (Msi-1) antibody (14H1) 1 : 200, mouse monoclonal anti-β-tubulin III antibody, 1 : 200 (Chemicon) mouse monoclonal PSA-NCAM, 1:200 (Pharmingen, San Jose, CA), and mouse monoclonal anti human BCL-2 antibody (Dako, 1 : 200). Sections were incubated with appropriate secondary donkey antibodies conjugated to FITC or rhodamine (Chemicon, 1 : 200) for 90 min at room temperature, and visualized or photographed with a confocal microscopy system (Zeiss LSM-510).

TUNEL Staining

To identify cells apoptosis, TUNEL labeling was carried out. Brain was removed rapidly en bloc and quickly frozen in liquid N_2 vapor. Sections 14 μm thick were cut on a cryostat and post-fixed in 1% PFA for 10 min. The Apoptag Fluorescein In Situ Apoptosis Detection Kit (S7110; Chemicon) was then applied. For immuno fluorescein-double labeling of TUNEL signal and BrdU, the TUNEL-fluorescein labeling was carried out first, followed by incubation in 2N HCl for 30 min at 37°C, and application of a rat monoclonal anti-BrdU antibody.

Transient Forebrain Ischemia

General anesthesia was maintained with 1% halothane. A column for measurement of cortical microperfusion by Laser-Doppler flowmetry (advanced laser flowmetry) was attached to the skull. Body and skull temperature were monitored and maintained at 36.5°C to 37.5°C. Both common carotid arteries were occluded for 12 min with microaneurysm clips and then reperfused. As described previously, only mice that showed <13% of baseline control microperfusion during the first minute of occlusion were used (Kitagawa et al., 1998). To examine the profiles of newborn neurons after ischemia, we injected BrdU (50 mg/kg, i.p.) 9 days after ischemia reported previously (Sasaki et al., 2003). As in normal conditions, BrdU was given four times every 2 hr. Thereafter, mice subjected to ischemia were processed under the same schedule as normal condition (each time-point 1, 4, 7, 14, and 30 days after BrdU administration).

Western Blotting

Samples of the hippocampus and the cortex of both NSE-bcl-2 transgenic mice and wild-type littermates were isolated. Proteins were separated by SDS-PAGE and transferred electrophoretically to polyvinylidene difluoride sheet (Immunobilon P; Millipore, Bedford, MA). Blots were probed with a mouse monoclonal bcl-2 antibody (Santa Cruz Biotechnology; 1 : 1,000), and a mouse monoclonal human bcl-2 antibody (Dakocytomation; 1 : 1,000), then detected using sheep anti-mouse HRP-conjugated secondary antibody (Amersham Pharmacia Biotech, Buckinghamshire, UK) followed by enhanced chemoluminescence (ECL; Amersham Pharmacia Biotech).

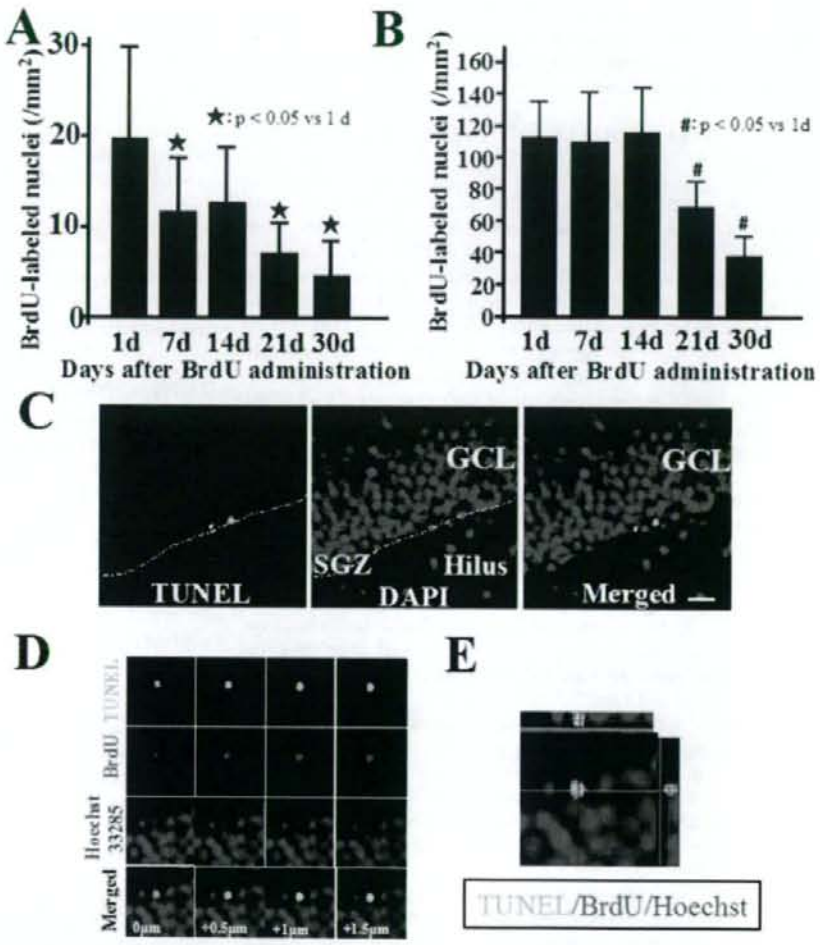

Fig. 1. Temporal profiles of BrdU-positive cells in normal (**A**) and ischemia (**B**) (n = 6). $^{\#,\star}P < 0.05$ vs. 1 day. **C:** TUNEL staining under normal condition in the dentate gyrus. Scale bar = 20 μm. **D,E:** At 21 days after BrdU administration, some of BrdU-positive cells showed TUNEL-positive, with the blue nuclear counterstain Hoechst 33258. Higher magnification views of selected individual z-planes (D) and a Z-series through the section (Z-distance = 10 μm) (E).

Neuron–Glia Mixed Cultures

To evaluate the direct effect of Bcl-2 on survival of newborn hippocampal neurons, primary hippocampal cultures from NSE-bcl-2 transgenic mice and their littermates were analyzed as described previously (Fujioka et al., 2004). The production of most hippocampal neuron is completed before birth in the mouse (between E15–E17), however, 85% of the hippocampal granular neurons in the dentate gyrus are generated postnatally (Bayer, 1980). It is widely known that granular neurons in the dentate gyrus show turnover throughout adulthood. Based on these findings, to directly confirm the findings that overexpression of BCL-2 enhanced the survival of nascent neurons in vivo, we carried out primary hippocampal culture with BrdU labeling at P0. To identify newborn neurons, BrdU (100 mg/kg, i.p.) was administered to P0 neonatal mice twice over 2 hr, and the hippocampus were dissected on P1 into HBSS without calcium or magnesium. Cells were dissociated with 1% trypsin (Invitrogen) and plated onto 6-cm dishes coated with Matrigel (BD Biosciences). Cells at a final concentration of 5×10^5 cells/ml were cultured in high-glucose DMEM (Sigma) containing 10% fetal calf serum. Twelve hours after seeding, the medium was changed to neuro basal medium supplemented with B-27 (Life Technologies), L-glutamine, 100 IU/ml penicillin, and 100 μg/ml streptomycin. Cells were cultured at 37°C in a humidified atmosphere of 95% air and 5% CO_2. These cultures contained neurons and astrocytes. After 13–15 days, the neurons in these cultures sit on the top of a confluent monolayer of astrocytes. At 1, 7, 14, and 30 days after seeding, cells were fixed immediately with 4% PFA for 30 min. Cells were then incubated with primary antibody at 4°C overnight. The slides were washed in three changes of phosphate-buffered saline, incubated with appropriate secondary donkey antibodies conjugated to FITC or rhodamine (Chemicon, 1 : 200) for 90 min at room temperature, and visualized or photographed with a confocal microscopy system (Zeiss LSM-510). The number of Tuj-1-positive neurons and Tuj-1/BrdU double-positive cells was counted in a field of 1 cm^2.

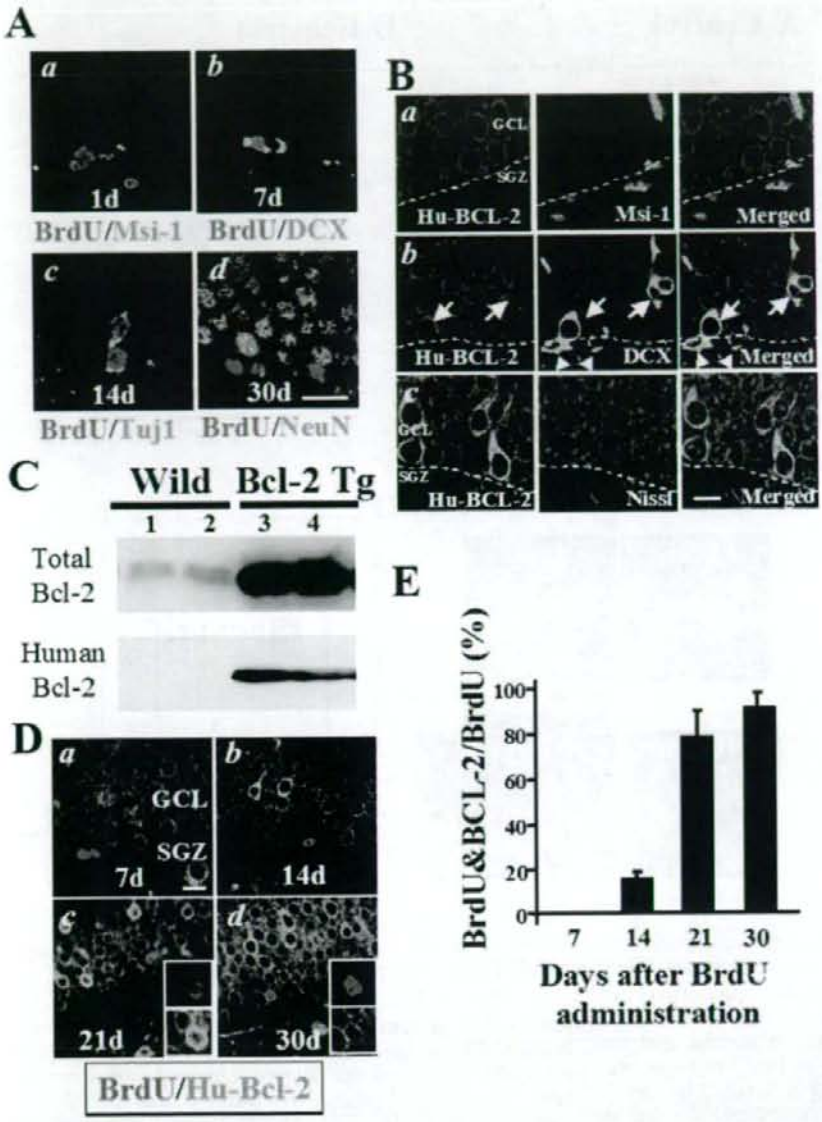

Fig. 2. **A:** Double-immunofluorescence staining of BrdU/Msi-1, BrdU/DCX, BrdU/Tuj1, and BrdU/NeuN was carried out. **B:** Expression of human Bcl-2 in NSE-*bcl-2* transgenic mice. **C:** Western blots analysis of total Bcl-2 and Human Bcl-2. Lane 1, hippocampus; lane 2, cortex ; lane 3, hippocampus; lane 4, cortex. **D,E:** Time course of human Bcl-2 immunoreactivity in BrdU-positive newborn neurons. Right insets in (C) show confocal images for BrdU (red) and Bcl-2 (green) from NSE-*bcl-2* transgenic mice (D) (n = 5). Scale bar = 20 μm (A), 10 μm (B), 30 μm (D).

Statistics

Data in the text and figures were described mean ± SD. Multiple comparisons were evaluated statistically by the analysis of variance, followed by Scheffé's post-hoc tests.

RESULTS

Survival of Newborn Cells in the Dentate Gyrus Under Normal and Ischemic Conditions

We determined the number of BrdU-positive cells and the phenotype of postmitotic cells at 1, 7, 14, 21, and 30 days after BrdU administration. Under normal conditions, the number of BrdU-positive cells showed a progressive reduction (1, 7, 14, 21, and 30 days; 19.7 ± 10.9, 11.3 ± 6.8, 12.3 ± 8.4, 8.7 ± 4.3, 4.8 ± 4.6/mm^2, respectively) (Fig. 1A). Next, we used double-immunolabeling with BrdU antibody and Msi-1 for neuronal progenitors, DCX for migrating neuroblast and immature neurons, Tuj1 for immature neurons, or NeuN for mature neurons (Fig. 2A). Most BrdU-positive cells in the SGZ showed Msi-1 staining 1 day after BrdU administration (Fig. 2Aa). Staining for DCX in BrdU-positive cells

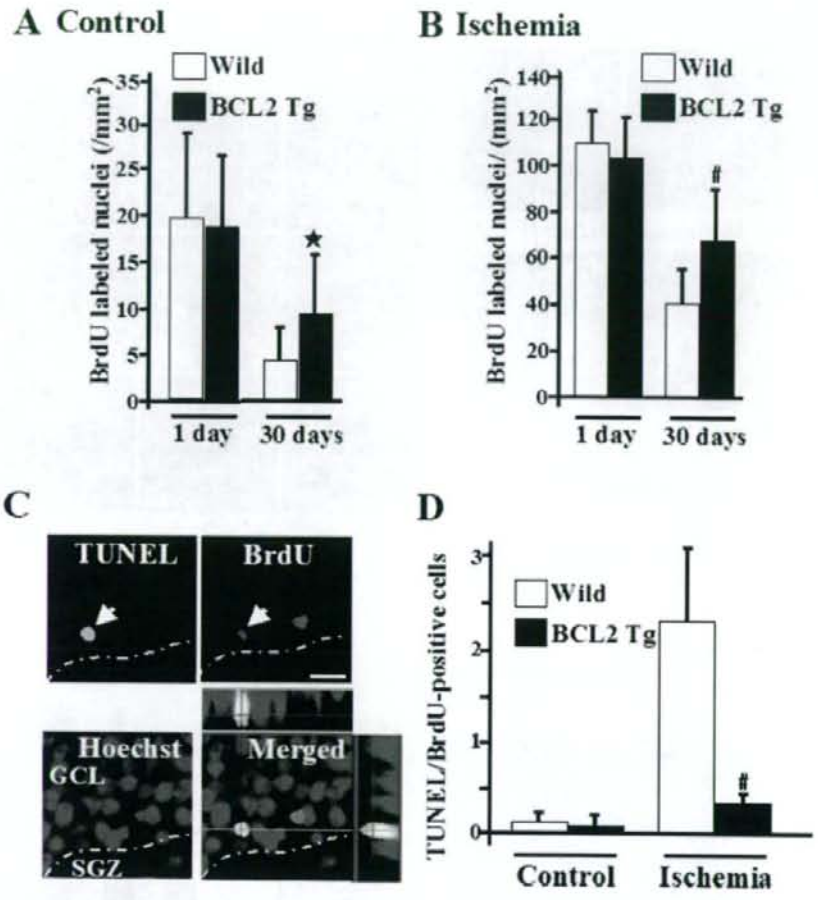

Fig. 3. Bcl-2 overexpression enhanced survival of hippocampal newborn neurons under normal (**A**) (n = 7) and ischemic conditions (**B**) (n = 8). **C,D:** Colocalization of TUNEL staining and BrdU after ischemia was shown (C, arrow), (Z-distance is 20 μm). Scale bar = 20 μm. **D:** Quantification of apoptosis of newborn neurons under normal and ischemic conditions. The number of BrdU/TUNEL double-positive cells at 21 days after BrdU administration was counted (n = 10). $^{\#}P < 0.05$ vs. normal.

peaked at 7–14 days, but declined dramatically 30 days after BrdU injection. BrdU-positive cells showing DCX or Tuj1 staining over time were similar (Fig. 2Ab,c). In contrast, BrdU/NeuN double-positive cells in the GCL were rare at 14 days after BrdU administration, and increased thereafter, and the majority of BrdU-positive cells showed NeuN staining at 30 days (Fig. 2Ad). The switch from expression of DCX or Tuj1 to NeuN seemed to occur between 14–30 days. Under ischemic conditions, there was no significant difference between the number of cells at 1 day and 14 days, thereafter, the numbers of BrdU-positive cells gradually declined up to 30 days (1, 7, 14, 21, and 30 days; 115.5 ± 23.7, 114.5 ± 30.5, 120.9 ± 32.9, 68.2 ± 13.0, and 38.7 ± 13.1/mm^2; Fig. 1B). To evaluate the contribution of apoptotic cell death to the progressive reduction in newborn cells, we used double-immunolabeling with anti-BrdU antibody and TUNEL staining. TUNEL-positive cells were detected in the SGZ and the inner layer of the GCL (Fig. 1C). Some of TUNEL-positive cells were also BrdU-positive at 21 days after BrdU administration (Fig. 1D,E).

Expression of the Human Bcl-2 Transgene During Adult Hippocampal Neurogenesis

Western blot analysis showed that the amount of total bcl-2 protein including both endogenous mouse bcl-2 and transgene human bcl-2 in NSE-*bcl-2* transgenic mice was augmented significantly compared to that in wild-type. Human bcl-2 protein was detected only in NSE-*bcl-2* transgenic mice (Fig. 2C). Double-immunolabeling with the antibody that recognized only human bcl-2 was carried out (Fig. 2B,D,E). To examine the expression of human Bcl-2 in NSE-*bcl-2* transgenic mice, double-immunofluorescence was carried out (Fig. 2B). Msi-1-positive cells in the SGZ did not stain for Bcl-2 (Fig. 2Ba). DCX- positive cells in the SGZ did not show immunostaining for Bcl-2 (Fig. 2Bb, arrowheads). In contrast, immature neurons within the GCL, as they migrated from the inner toward the outer layer, showed colocalization of DCX and Bcl-2 (Fig. 2Bb, arrows). Most Nissl-positive mature neurons showed Bcl-2 staining (Fig 2Bc). Expression of the transgene was rarely detected as early as 14 days after BrdU administration, but increased in number thereafter and

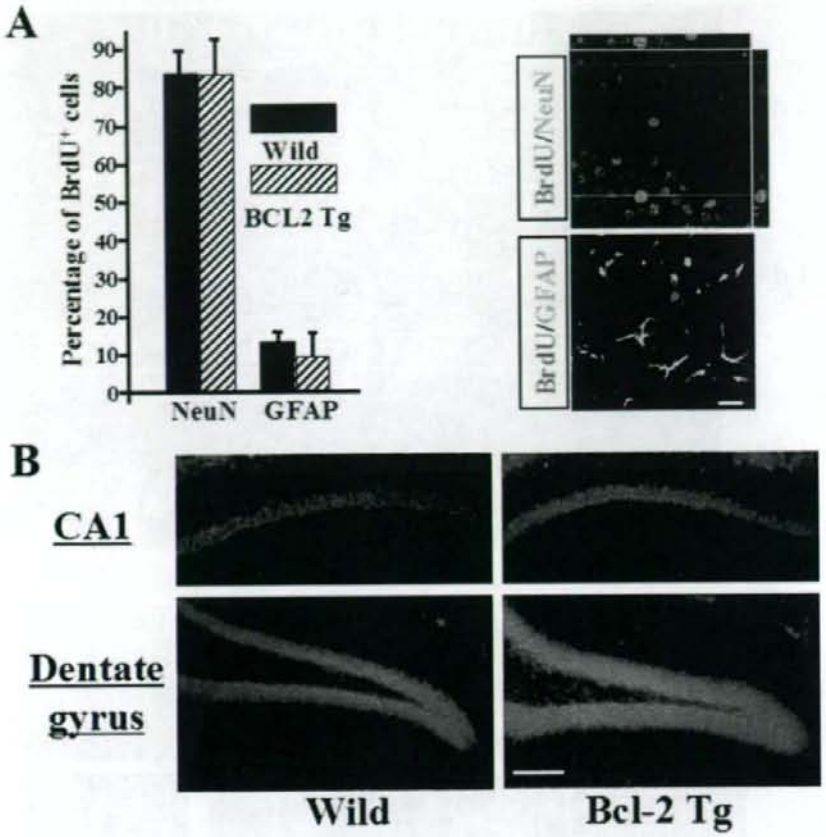

Fig. 4. **A:** We examined the effect of bcl-2 overexpression on the differentiation of newborn neurons. **B:** Total volume of cells in the hippocampal CA1 sector (upper panel) or in the dentate gyrus (lower panel) of NSE-*bcl-2* transgenic mice and wild-type littermates in the 18-month-old mouse. Scale bar = 30 μm (B), 100 μm (C).

became stable (Fig. 2Da–d). Semiquantitative analysis of BrdU/Bcl-2 double-positive cells were 0% at 7 days, 15.8 ± 3.2% at 14 days, 79.1 ± 10.3% at 21 days, and 88.6 ± 7.0% at 30 days (Fig. 2D,E). These findings indicated that human-*bcl-2* gene expression under the control of the NSE promoter began at the immature neuronal stage and remained constant in surviving mature neurons.

Progenitor Cell Proliferation, Survival, and Differentiation in NSE-bcl-2 Transgenic Mice

There were no significant differences in any of the parameters including cerebral blood flow, rectal and skull temperatures between both groups during and after transient forebrain ischemia (data not shown). Under normal conditions, no significant differences between NSE-*bcl-2* transgenic mice (18.5 ± 8.0/mm^2) and wild-type littermates (19.5 ± 10.8/mm^2) were observed in the number of BrdU-positive cells at 1 day after BrdU administration (Fig. 3A). Survival of progenitor cells was examined 30 days after BrdU administration. The numbers of BrdU-positive cells were 4.5 ± 3.5/mm^2 in wild-type littermates and 9.5 ± 7.1/mm^2 in NSE-*bcl-2* transgenic mice (Fig. 3A). Compared to the values obtained at Day 1, the number of surviving BrdU-positive cells was greater in NSE-*bcl-2* transgenic mice (51%) than in wild-type littermates (24%), with an approximate 25% increase. The numbers of BrdU/NeuN double-positive cells were 4.0 ± 2.8/mm^2 in wild-type littermates and 8.4 ± 5.6/mm^2 in NSE-*bcl-2* transgenic mice. The ischemic neuronal damage in the hilus was of similar severity between NSE-*bcl-2* transgenic mice and wild-type littermates, and the survival of newborn granule neurons was not associated with the degree of the injury of the CA1 sector (data not shown). After ischemia, the number of BrdU-positive cells at Day 1 did not differ between NSE-*bcl-2* transgenic mice (100.5 ± 21.1/mm^2) and wild-type littermates (110.9 ± 15.8/mm^2). The number of BrdU-positive cells 1 day after BrdU labeling was not different between both groups at 39 days (10.8 ± 7.4/mm^2 in wild-type littermates; 8.2 ± 6.8/mm^2 in NSE-*bcl-2* transgenic mice) after ischemia. In contrast, NSE-*bcl-2* transgenic mice (65.7 ± 26.7/mm^2) showed a significant increase in the number of BrdU-positive cells in the SGZ and GCL compared to that in wild-type littermates (41.0 ± 17.6/mm^2), an approximate 30% increase in survival rate (Fig. 3B). Moreover, the number

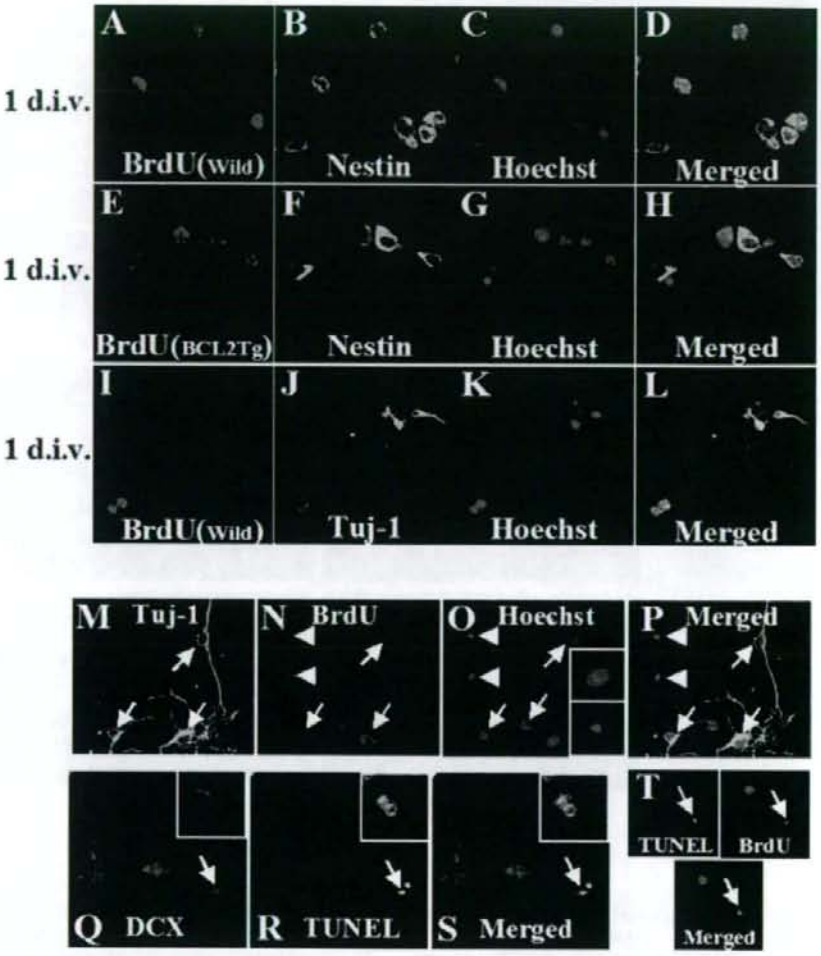

Fig. 5. BrdU (red), nestin (green), and Hoechst 33285 (blue) fluorescence of wild-type littermates (**A–D**) and NSE-*bcl-2* transgenic mice (**E–H**) at 1 day after seeding were shown. A merged image of (D) and (H) depicts BrdU/nestin/Hoechst. **I–L:** BrdU, Tuj-1, and Hoechst fluorescence at 1 day were visualized. **M–P:** Nuclear morphology of BrdU-positive newborn cells in primary culture 14 days after seeding visualized by Hoechst staining. Nuclear morphology with healthy-looking chromatin structure in BrdU/Tuj-1 double-positive cells (arrows) was visualized by Hoechst (O, right insets, upper panel). In contrast, some of BrdU-positive newborn neurons had fragmented and condensed nuclei (arrowheads) (O, right insets, bottom panel). **Q–S:** DCX and TUNEL fluorescence were shown (DCX/TUNEL double-positive cells; arrow). **T:** TUNEL/BrdU double-positive cells (arrows) were visualized.

of BrdU/NeuN double-positive cells in NSE-*bcl-2* transgenic mice (56.5 ± 18.7/mm^2) was significantly increased than that in wild-type littermates (36.1 ± 12.3/mm^2).

To assess the contribution of apoptotic cell death to the progressive reduction, we used double-immunolabeling with anti-BrdU antibody and TUNEL staining. Some of BrdU-positive cells showed colocalization of TUNEL staining (Fig. 3C, arrow). Under ischemic condition, the number of BrdU/TUNEL double-positive cells in NSE-*bcl-2* transgenic mice (0.3 ± 0.1/section, n = 10) was significantly decreased than that in wild-type littermates (2.3 ± 1.0/section, n = 10) (Fig. 3C,D). This finding suggests that ischemia promotes the proliferation of newborn cells. Followed by the increased number of death of newborn cells, however, Bcl-2 overexpression enhanced survival of those newborn neurons.

Under both conditions, no significant differences were observed in the percentages of BrdU/NeuN double-positive cells and BrdU/GFAP double-positive cells in the SGZ and GCL between the groups at 30 days (Fig. 4A). Under ischemic conditions, no significant differences were observed in progenitor cell differentiation (data not shown). There was no significant difference in the total volume of the hippocampal CA1 sector in the 18-month-old mouse. On the other hand, the total volume of cells in the DG in NSE-*bcl-2* transgenic mice was significantly greater than that of wild-type littermates. These data provide additional evidence consistent with the reduced cell death by Bcl-2 transgene (Fig. 4B).

Enhanced Survival of Newborn Neurons From NSE-bcl-2 Transgenic Mice in Neuron–Glia Mixed Culture

To directly confirm the findings that Bcl-2 enhanced survival of nascent neurons in vivo, we analyzed primary

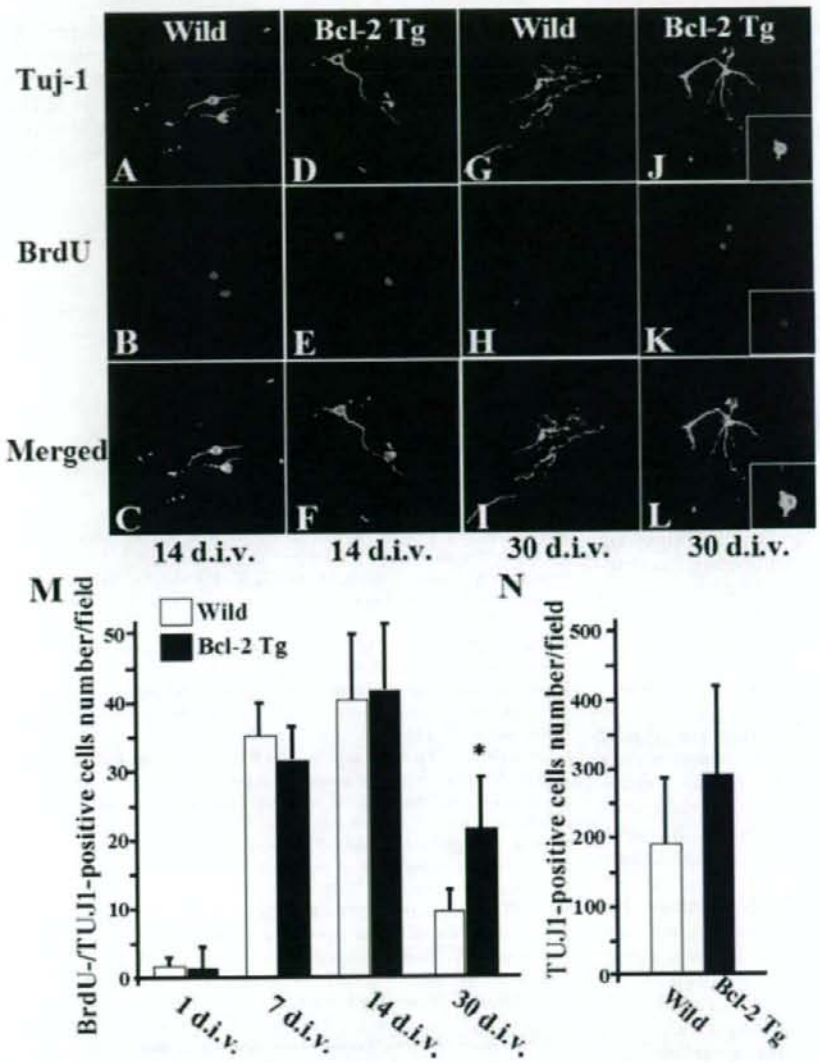

Fig. 6. Effect of Bcl-2 overexpression on survival of newborn neurons in primary neuron-glia culture. **A–L:** High-magnification confocal images are shown for Tuj1 (green) and BrdU (red) of cultured primary hippocampal neurons from wild-type littermates (A–C, G–I) and NSE-*bcl-2* transgenic mice (D–F, J–L) at 14 days (A–F) or 30 days (G–L) after seeding (L). Right insets in (J–L) show Bcl-2 immunofluorescence (green) in BrdU-positive hippocampal neurons (red) from NSE-*bcl-2* transgenic mice at 30 days. The number of Tuj1/BrdU double-positive cells (**M**) and the total number of BrdU-positive cells (**N**) at 30 days ($n = 8$). $*P < 0.05$ vs. control. Figure can be viewed in color online via www.interscience.wiley.com.

hippocampal cultures from P0 mice with BrdU labeling. In our hippocampal cultures, >90% of BrdU-positive cells were positive for the precursor cell marker nestin in wild-type littermates and in NSE-*bcl-2* transgenic mice at 1 day after seeding (Fig. 5A–H). In contrast, only a few BrdU-positive cells showed expression for the neuronal marker Tuj1 at 1 day (Fig. 5I–L). The nuclear morphology of neurons was examined after staining the cell nuclei with Hoechst 33285 dye. Newborn neuronal identity of the cells was shown by double-labeling for BrdU and Tuj-1. After 14 days, many BrdU/Tuj-1 double-positive newborn neurons displayed typical, healthy-looking, chromatin structure (Fig. 5M–P, arrows). Some of newborn neurons had fragmented and condensed nuclei (Fig. 5M–P, arrowheads). Moreover, some of DCX-positive immature neurons were TUNEL-positive (Fig. 5Q–S, arrowheads). No differences between two groups were observed in the numbers of cultured BrdU/Tuj-1 double-positive new neurons at 1, 7, or 14 days after seeding (Fig. 6A–L). In contrast, NSE-*bcl-2* transgenic mice showed a significant increase in the numbers of cultured BrdU/Tuj-1 double-positive cells compared to the numbers of wild-type littermates at 30 days (1, 7, 14, and 30 days in wild-type: 1.8 ± 0.1, 36.2 ± 3.3, 41.1 ± 9.0, 9.8 ± 3.1, respectively; in NSE-*bcl-2* transgenic mice: 1.6 ± 0.4, 30.8 ± 3.4, 42.4 ± 9.6, 22.3 ± 7.3, respectively) (Fig. 6M). There was an

increase in the total number of Tuj1-positive neurons in NSE-*bcl-2* transgenic mice at 30 days ($P = 0.09$) (Fig. 6N). These results showed that Bcl-2 expression promotes survival of cultured newborn neurons.

DISCUSSION

The present findings provide insight into the role of Bcl-2 in adult neurogenesis. Consistent with previous studies (Young et al., 1999), most newborn cells, a mixed population of immature and mature neurons, die via apoptosis. It has been reported recently that in the adult mouse olfactory bulb, Days 14–28 after the generation are a critical period for the survival of new granule cells, and during that time they become susceptible to apoptotic cell death (Yamaguchi and Mori, 2005). This study shows that almost the same time-point was crucial for the survival of newborn neurons in the adult hippocampus under ischemic conditions.

In the CNS, Bcl-2 is expressed highly during neurogenesis in the developing brain. Bcl-2 plays important roles in the regulation of neuronal death during development and the early postnatal period (Martinou et al., 1994). Moreover, in the hippocampal dentate gyrus, Bcl-2 expression is high not only during development but also in adulthood (Merry et al., 1994).

Consistent with the study by Fujioka et al. (2004), we also observed that, in addition to mature granule cells, newborn immature neurons in the dentate gyrus of *bcl-2* transgenic mice under the NSE promoter expressed human Bcl-2 immunoreactivity (Fig. 2). Aged NSE-*bcl*-2 transgenic mice possess supernumerary neurons in the dentate gyrus, but not in the CA1 and CA2 subregions. Based on these findings, we used NSE-*bcl*-2 transgenic mice to elucidate the role of Bcl-2 in adult neurogenesis.

TUNEL staining indicates simply DNA damage, but it is not a specific marker of apoptosis. Therefore, we must interpret TUNEL staining vigilantly. BrdU labeling is necessary, but not sufficient, to prove that a given cell has divided. Bauer and Patterson (2005) showed recently that BrdU is not incorporated significantly during DNA repair in three models of injury-induced neuronal apoptosis.

Cerebral ischemia leads to markedly enhanced proliferation of neuronal progenitor cells (Liu et al., 1998; Yagita et al., 2001). However, only a small fraction of these newborn neurons survive. We observed that ischemia induced a similar increase in both BrdU-positive cells and BrdU/TUNEL double-positive cells in the hippocampal dentate gyrus. The present study suggests that ischemia simultaneously increases both neurogenesis and neuronal elimination and that Bcl-2 is important for the long-term survival of newborn neurons in hippocampal neurogenesis after ischemia. Additionally, the Bcl-2 family has been shown to be important for protection from focal and global ischemia (Martinou et al., 1994; Kitagawa et al., 1998). The ability to upregulate Bcl-2 expression may lead to the development of brain protection and repair strategies for the treatment of brain ischemia.

In summary, this study shows that Bcl-2 overexpression increases survival of newly generated neurons in the hippocampal dentate gyrus under normal and ischemic conditions. These results indicate that modulation of Bcl-2 levels may have implications for therapeutic intervention to enhance neurogenesis for functional restoration, particularly after ischemia.

ACKNOWLEDGMENTS

The authors thank A. Kanzawa and S. Higa for secretarial assistance. T. Sasaki is a research fellow of the Japan Society of the Promotion of Science.

REFERENCES

Abe-Dohmae S, Harada N, Yamada K, Tanaka R. 1993. Bcl-2 gene is highly expressed during neurogenesis in the central nervous system. Biochem Biophys Res Commun 191:915–921.

Adams JM, Cory S. 1998. The Bcl-2 protein family: arbiters of cell survival. Science 281:1322–1326.

Arvidsson A, Collin T, Kirik D, Kokaia Z, Lindvall O. 2002. Neuronal replacement from endogenous precursors in the adult brain after stroke. Nat Med 8:963–970.

Bauer S, Patterson PH. 2005. The cell cycle-apoptosis connection revisited in the adult brain. J Cell Biol 171:641–650.

Bayer SA. 1980. Development of the hippocampal region in the rat. I. Neurogenesis examined with 3H-thymidine autoradiography. J Comp Neurol 190:87–114.

Chen J, Graham SH, Nakayama M, Zhu RL, Jin K, Stetler RA, Simon RP. 1997. Apoptosis repressor genes Bcl-2 and Bcl-x-long are expressed in the rat brain following global ischemia. J Cereb Blood Flow Metab 17: 2–10.

Fujioka T, Fujioka A, Duman RS. 2004. Activation of cAMP signaling facilitates the morphological maturation of newborn neurons in adult hippocampus. J Neurosci 24:319–328.

Gould E, Cameron HA. 1996. Regulation of neuronal birth, migration and death in the rat dentate gyrus. Dev Neurosci 18:22–35.

Kempermann G, Gast D, Kronenberg G, Yamaguchi M, Gage FH. 2003. Early determination and long-term persistence of adult-generated new neurons in the hippocampus of mice. Development 130:391–399.

Kitagawa K, Matsumoto M, Tsujimoto Y, Ohtsuki T, Kuwabara K, Matsushita K, Yang G, Tanabe H, Martinou JC, Hori M, Yanagihara T. 1998. Amelioration of hippocampal neuronal damage after global ischemia by neuronal overexpression of BCL-2 in transgenic mice. Stroke 29:2616–2621.

Liu J, Solway K, Messing RO, Sharp FR. 1998. Increased neurogenesis in the dentate gyrus after transient global ischemia in gerbils. J Neurosci 18:7768–7778.

Martinou JC, Dubois-Dauphin M, Staple JK, Rodriguez I, Frankowski H, Missotten M, Albertini P, Talabot D, Catsicas S, Pietra C, et al. 1994. Overexpression of BCL-2 in transgenic mice protects neurons from naturally occurring cell death and experimental ischemia. Neuron 13: 1017–1030.

Merry DE, Veis DJ, Hickey WF, Korsmeyer SJ. 1994. bcl-2 protein expression is widespread in the developing nervous system and retained in the adult PNS. Development 120:301–311.

Pencea V, Bingaman KD, Wiegand SJ, Luskin MB. 2001. Infusion of brain-derived neurotrophic factor into the lateral ventricle of the adult rat leads to new neurons in the parenchyma of the striatum, septum, thalamus, and hypothalamus. J Neurosci 21:6706–6717.

Sasaki T, Kitagawa K, Sugiura S, Omura-Matsuoka E, Tanaka S, Yagita Y, Okano H, Matsumoto M, Hori M. 2003. Implication of cyclooxygenase-2 on enhanced proliferation of neural progenitor cells in the adult mouse hippocampus after ischemia. J Neurosci Res 72:461–471.

van Praag H, Kempermann G, Gage FH. 1999. Running increases cell proliferation and neurogenesis in the adult mouse dentate gyrus. Nat Neurosci 2:266–270.

van Praag H, Schinder AF, Christie BR, Toni N, Palmer TD, Gage FH. 2002. Functional neurogenesis in the adult hippocampus. Nature 415:1030–1034.

Yagita Y, Kitagawa K, Ohtsuki T, Takasawa K, Miyata T, Okano H, Hori M, Matsumoto M. 2001. Neurogenesis by progenitor cells in the ischemic adult rat hippocampus. Stroke 32:1890–1896.

Yamaguchi M, Mori K. 2005. Critical period for sensory experience-dependent survival of newly generated granule cells in the adult mouse olfactory bulb. Proc Natl Acad Sci U S A 102:9697–9702.

Young D, Lawlor PA, Leone P, Dragunow M, During MJ. 1999. Environmental enrichment inhibits spontaneous apoptosis, prevents seizures and is neuroprotective. Nat Med 5:448–453.